

Aluminum Nitride in Al–Si–Mg Alloy

Arya, Samira M.; Griffiths, W. D.

DOI:

[10.1007/s11663-023-02810-8](https://doi.org/10.1007/s11663-023-02810-8)

License:

Creative Commons: Attribution (CC BY)

Document Version

Publisher's PDF, also known as Version of record

Citation for published version (Harvard):

Arya, SM & Griffiths, WD 2023, 'Aluminum Nitride in Al–Si–Mg Alloy', *Metallurgical and Materials Transactions B*, vol. 54, no. 4, pp. 1965-1984. <https://doi.org/10.1007/s11663-023-02810-8>

[Link to publication on Research at Birmingham portal](#)

General rights

Unless a licence is specified above, all rights (including copyright and moral rights) in this document are retained by the authors and/or the copyright holders. The express permission of the copyright holder must be obtained for any use of this material other than for purposes permitted by law.

- Users may freely distribute the URL that is used to identify this publication.
- Users may download and/or print one copy of the publication from the University of Birmingham research portal for the purpose of private study or non-commercial research.
- User may use extracts from the document in line with the concept of 'fair dealing' under the Copyright, Designs and Patents Act 1988 (?)
- Users may not further distribute the material nor use it for the purposes of commercial gain.

Where a licence is displayed above, please note the terms and conditions of the licence govern your use of this document.

When citing, please reference the published version.

Take down policy

While the University of Birmingham exercises care and attention in making items available there are rare occasions when an item has been uploaded in error or has been deemed to be commercially or otherwise sensitive.

If you believe that this is the case for this document, please contact UBIRA@lists.bham.ac.uk providing details and we will remove access to the work immediately and investigate.

Aluminum Nitride in Al–Si–Mg Alloy



SAMIRA M. ARYA and W.D. GRIFFITHS

When liquid aluminum is exposed to air, an oxide layer instantaneously forms on the surface of the melt, which, when enfolded, becomes a double oxide film defect (bifilm), producing entrained air pockets forming voids, cracks, and areas of stress. Studies of the reactions between the air trapped inside the bifilms and the surrounding melt have produced reaction products such as AlN. In this study, examination of the fracture surfaces of an Al–7Si–0.3Mg (2L99) as-cast alloy revealed AlN apparently of a different “nodular” morphology of approximately 15 μm in length. In contrast to the “feather-shaped” AlN morphology grown through holding in nitrogen or the addition of Mo to 2L99 observed in previous research, the observed nodular morphology in this study was thought to be less permeable. This confirmed the hypothesis of Nyahumwa *et al.* (AFS Trans 106:215–223, 1998), who suggested that the entrapped air in bifilms can react with the surrounding liquid melt by initially consuming oxygen to form oxides, such as spinel (MgAl_2O_4), followed by the consumption of the nitrogen to form AlN. The AlN observed has been proposed to reduce the size of bifilms and correspondingly improve the mechanical properties of the alloy. In this work, AlN was also grown by holding alloys in a controlled nitrogen gas environment at 850 °C at various holding times to reveal AlN morphologies.

<https://doi.org/10.1007/s11663-023-02810-8>
© The Author(s) 2023

I. INTRODUCTION

ALUMINUM alloys are widely used in the aerospace and automotive industries owing to their castability and high strength-to-weight ratio. During the casting process, liquid Al reacts with air to create a surface oxide layer almost instantaneously. Provided the oxide layer stays at the surface, it can be seen as beneficial as it protects the bulk liquid metal from further reaction. However, with any surface turbulence of the melt, the surface oxides can be entrained into the bulk liquid-forming double oxide film defects (bifilms) containing air or other mold gases^[1] (see Figure 1). The internal surfaces of the bifilms form as dry-side to dry-side crevices in the final casting, reducing the mechanical properties, fatigue, and areas of stress concentration.^[2]

Nyahumwa *et al.*^[2] studied the effects of surface turbulence during casting on the fatigue life of cast A356 (Al–7Si–Mg) commercial aluminum alloy, suggesting that the gradual consumption of the entrapped gases (air) in the bifilms was caused by the reaction of internal

gases with the surrounding liquid metal, as shown in Figure 2. They proposed that, initially, oxygen was consumed by reaction with the liquid metal to give spinel, followed by the reaction between the liquid metal and the entrapped N_2 to form AlN.

Apart from alumina, spinel, and MgO, AlON is a possible phase. However, Figure 3 shows a eutectoid Al_2O_3 –AlN phase diagram.^[3] The phase diagram shows that AlON is not to be expected to occur at temperatures below 1640 °C.^[3] At room temperature, AlON is not stable and only occurs at extremely restricted pressures of O and N of approximately 10^{-10} bar.^[4]

Nyahumwa *et al.*^[2] further suggested that the phase transformation of alumina from γ to α -alumina could cause a 24 pct reduction in the oxide volume and consequently cause a rupture of the oxide surface of the bifilm.

Impey *et al.*^[5] reported that the phase transformation from γ to α -alumina largely depended on the presence of water vapor associated with the humidity of the air and time. They reported that oxidation starts immediately, and the rate of oxidation reduces to a lower rate after 30 to 60 minutes. However, after approximately 5 hours, the breakaway transformation from gamma to alpha alumina occurs following hydrogen absorption, which leads to the natural removal of hydroxyl ions that function as a stabilizer for gamma alumina. The transformation is reported by Impey *et al.*^[5] to continue for up to 24 hours and is more pronounced in dry air.^[5] El Sayed *et al.*^[6] studied the rate of consumption of the

SAMIRA M. ARYA and W.D. GRIFFITHS are with the School of Metallurgy and Materials, College of Engineering and Physical Sciences, University of Birmingham, Edgbaston, Birmingham, B15 2TT, UK. Contact e-mail: sxm566@student.bham.ac.uk

Manuscript submitted October 10, 2022; accepted April 26, 2023.

Article published online May 22, 2023.

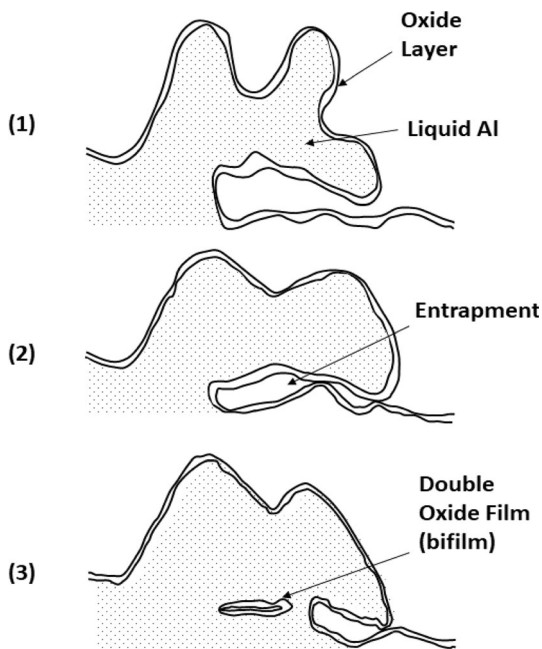


Fig. 1—Sketch of an oxide layer leading to entrapment and bifilms in Al melt. Reprinted from Ref. [1].

gases inside air bubbles in various alloys. They claimed that the type of oxide, which was in turn defined by the alloy composition, affected the consumption rate of oxygen and nitrogen and the rate of hydrogen diffusion into the bifilm. The time estimated for the consumption of O and N in a bifilm defect in Al–5Mg alloy was reported to be approximately 6 minutes, 9 minutes for CP–Al, and 25 minutes for 2L99, respectively.^[6]

The consumption of the internal gases proposed by Nyahumwa *et al.*^[2] was thought to begin a reaction with oxygen, forming Al_2O_3 in the case of pure Al, MgAl_2O_4 in the case of 2L99, or MgO in the case of Al–5Mg alloy, followed by nitrogen to form AlN. El Sayed *et al.*^[6] observed granular (described by them as nodular) AlN structures in CP–Al (held for 40 minutes) and 2L99 (held for 32 minutes) at 720 °C, as shown in Figures 4(a) and (b). Figures 4(c) and (d) show the EDX spectra, respectively. It was also reported that hydrogen might diffuse into the entrapped bifilm defects during their residence in the melt.^[6]

It is worth noting that aluminum nitride can form when liquid Al is reacted directly with nitrogen gas (Eq. [1]) in the production of a reinforced Metal Matrix Composite (MMC), obtained by blowing N gas into the melt at a pre-determined rate.^[7,8]



Zheng *et al.*^[9] reported having formed smaller than 10 μm spherical dendritic AlN particles by bubbling N_2 directly into a pure Al melt for 6 hours at 1200 °C.

Raeiszadeh and Griffiths^[10–12] studied the reaction rate of a trapped air bubble in pure (CP) liquid Al, using real-time X-ray radiography to record the changes in the volume of air when in contact with liquid Al at 850 °C. They concluded that all O was consumed within about the first 4 hours, followed by complete consumption of N for a further 4 hours (8 hours in total), forming feather-like nitrides of approximately 10 μm in length. Figure 5(a) shows an SEM micrograph of the AlN layer, and Figure 5(b) shows an EDX spectrum of the whole area of Figure 5(a).

Gerrard *et al.*^[13,14] also observed feather-shaped AlN on CP–Al, by first degassing a LECO sample to remove existing hydrogen from the metal, followed by heating the sample to above its melting point at 700 °C and holding it for 15 minutes in a nitrogen atmosphere, as shown in Figure 6(a). Figure 6(b) shows an EDX analysis of Figure 6(a). The composition of spectrum1 showed the presence of oxides at 5 wt pct, nitrides at 12 wt pct, and Fe at 2 wt pct.^[13,14]

Griffiths *et al.*^[15] studied the fracture surfaces of CP–Al, and Al–5Mg alloy and observed the whisker structure of alumina and magnesium oxide inside pores after 20 minutes of melt holding time. Their study suggested that the whisker shapes could have been formed due to the evaporation of oxides within the pores, followed by condensation. Chen and Griffiths^[16,17] also observed feather-shaped AlN, of about 14 μm thickness, on the fracture surface of 2L99 + 0.4 wt pct Mo alloy, cast at 730 °C, followed by a T6 heat treatment. They reported that, with the addition of 0.4 wt pct Mo to 2L99 alloy, the Weibull modulus of the Ultimate Tensile Strength (UTS) was increased from 277 to 304 MPa, and %Elongation increased from 2.1 to 3.6 pct.

The feather-shaped AlN morphology shown in Figure 7(a) was considered to be permeable, which could promote the consumption of the entrapped gases leading to a reduction in the sizes of the bifilms. As a result, a certain degree of bonding between the two un-wetted oxide surfaces might then occur, thereby improving the mechanical properties of the alloy. Figure 7(b) shows the EDX spectrum of the area marked in Figure 7(a). The EDX analysis of this area showed the presence of O at 9 at pct, N at 36 at pct, Si at 5 at pct, Al at 49.6 at pct, and Mg at 0.4 at pct.

A granular AlN structure was also reported by Chen and Griffiths on the surface of 2L99 + 0.4 wt pct Mo alloy using a trapped air bubble experiment. The sample was held for 1 hour at 725 °C (as shown in Figure 8(a)). The granular AlN structure shown in Figure 8(a) contrasts with the feather-shaped morphology presented

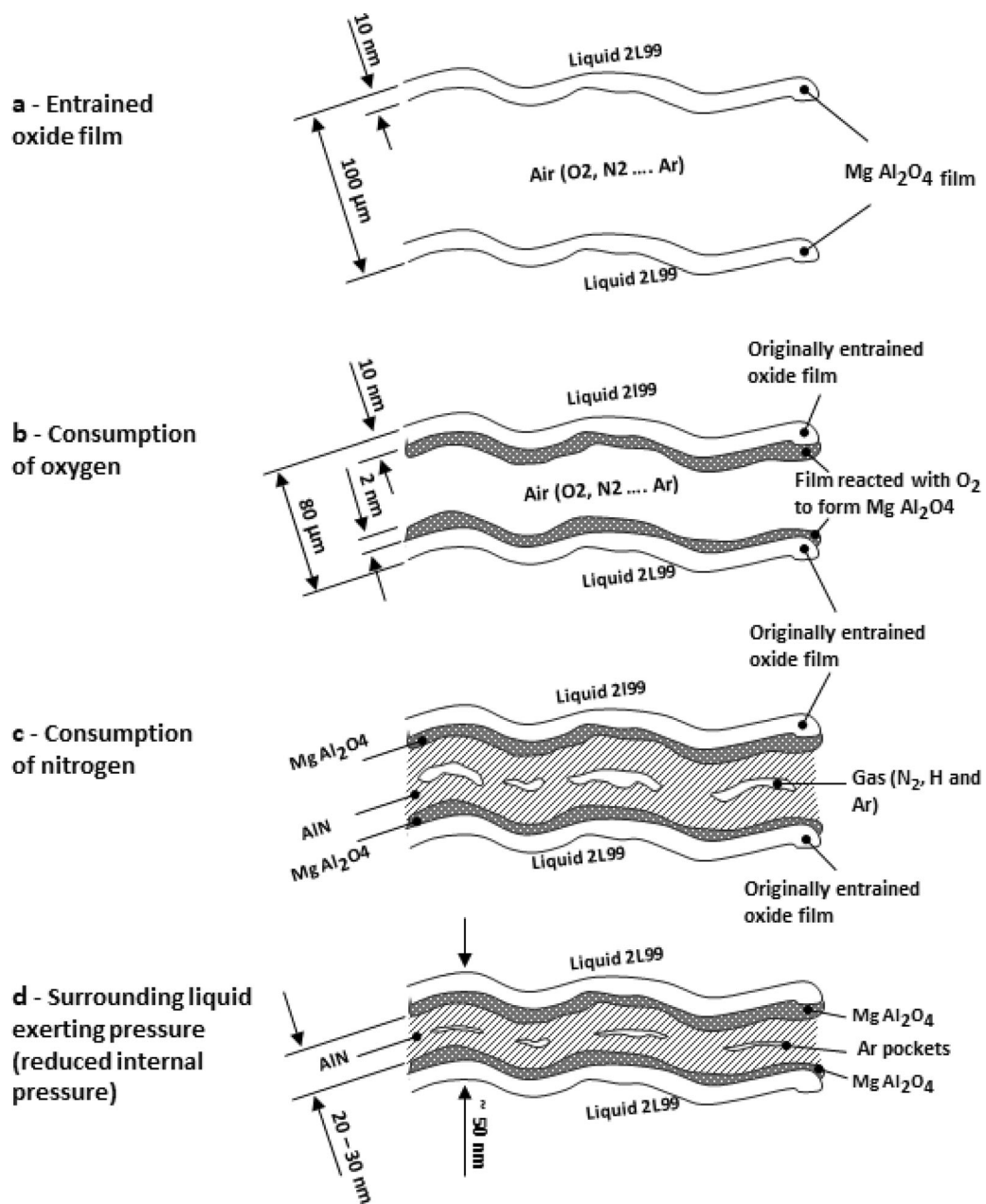


Fig. 2—Nyahumwa sketch of the conception of gases inside the bifilm in 2L99 alloy. Reprinted with permission from Ref. [2].

in Figure 7(a) and may be considered impermeable. Figure 8(b) shows the EDX spectrum for the area marked X1 in Figure 8(a).

Wang and Fan^[18] reported the characterization of nitride particles formed in CP-Al at 750 °C and 850 °C, as shown in Figures 9(a) and (b). Their characterization was conducted using analytical electron microscopy on samples derived from a pressure melt filtration technique using a Prefil-Footer printer device. The EDX

spectra are presented in Figure 9(c) for all particles marked in Figures 9(a) and (b). The morphology of the observed AlN particles was that of short (1 μm) rod-shaped objects, measured to be 104 nm and 375 nm in width and length, respectively. The observed AlN particles were described as hexagonal wurtzite AlN with a close-packed plane.^[18] Based on Figures 9(a) and (b), it might be concluded that the AlN particles may have nucleated on an oxide film.

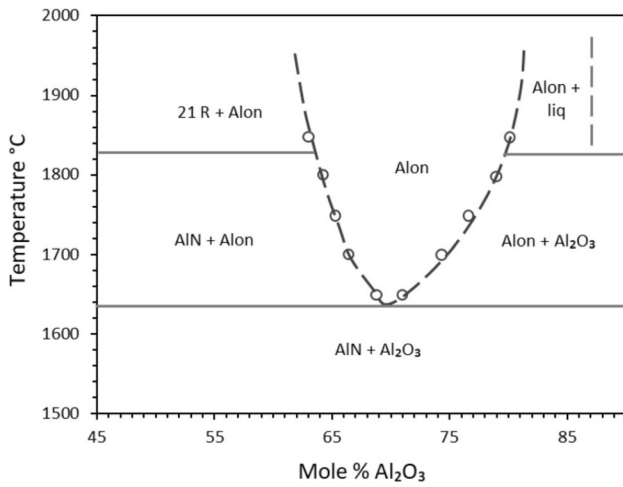


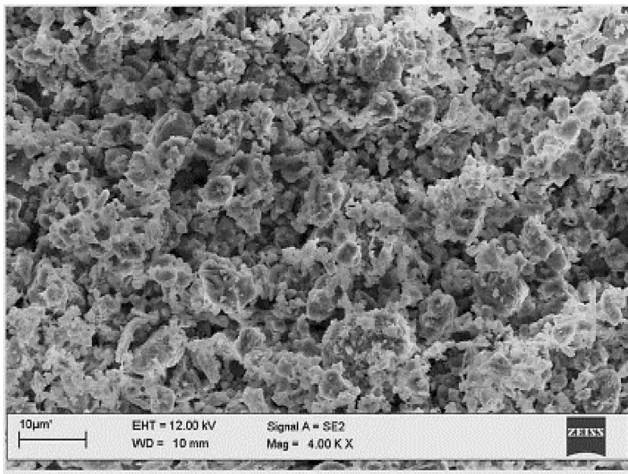
Fig. 3—Phase diagram of eutectoid Al₂O₃-AlN reprinted from Ref. [3].

Based on the crystallography of the observed AlN particles, they calculated the lattice matching potency of the particles as a nucleating substrate for α -Al grains, using Eqs. [2] and [3].

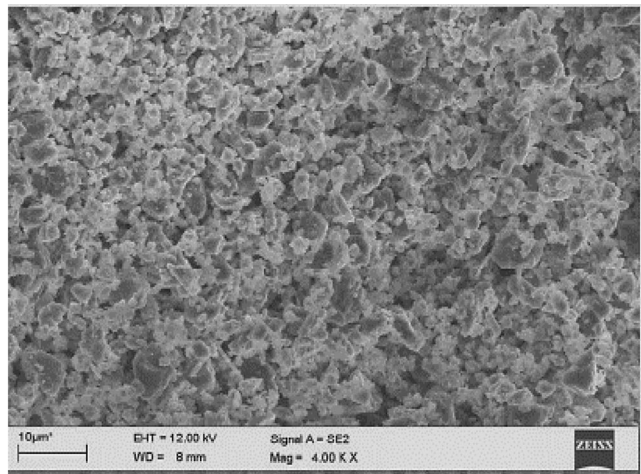
$$fr = rAl - rp * \frac{1}{rp} \times 100pct, \quad [2]$$

$$fd = dAl - dp * \frac{1}{dp} \times 100pct, \quad [3]$$

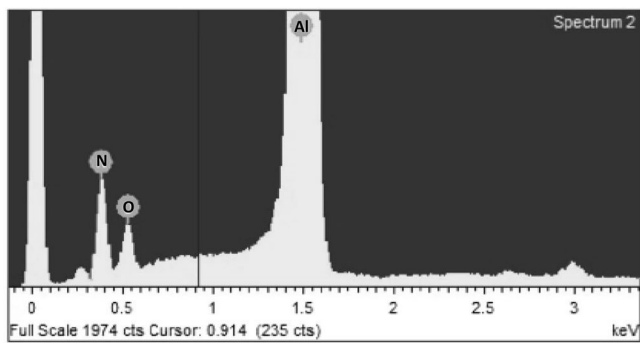
where rAl and rp are the interatomic spacings along the most close-packed directions, and dAl and dp are the interplanar spacings of the most close-packed planes of Al, oxides, borides, and AlN. fr represents the interatomic spacing misfit, and fd represents the interplanar misfit of close-packed planes. Wang and Fan^[18] calculated that the interatomic spacing misfit (see Table I) with the close-packed directions of the



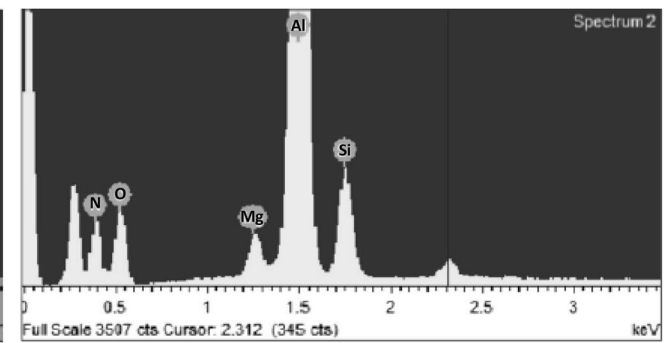
(a)



(b)



(c)



(d)

Fig. 4—(a) SEM micrograph shows granular AlN on CP-Al after 40 minutes holding time (b) SEM micrograph of granular AlN on 2L99 after 32 minutes holding time (c) and (d) EDX spectrum of (a) and (b). Reprinted from Ref. [6].

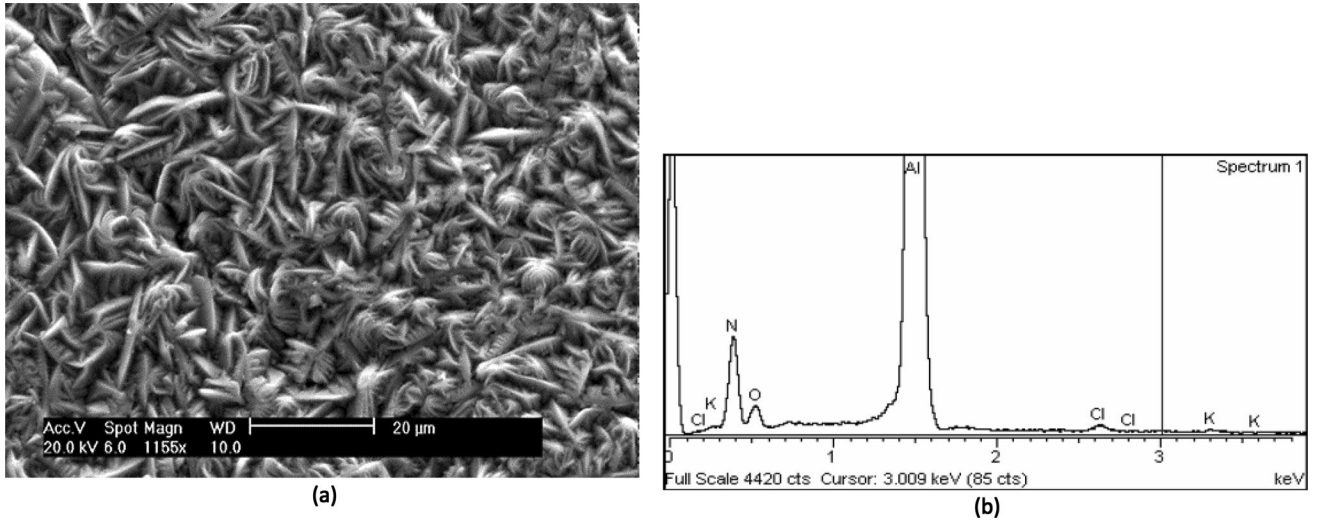


Fig. 5—(a) SEM micrograph of feather AlN layer (b) EDX spectrum of the whole area of (a). Reprinted from Refs. [10–12].

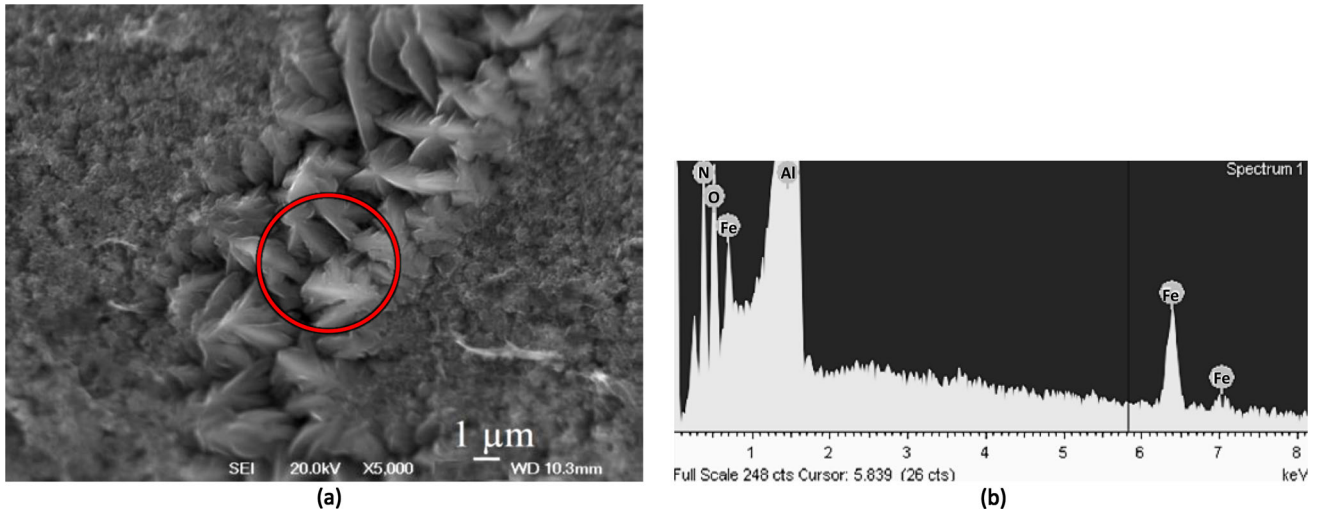


Fig. 6—(a) SEM micrograph of feather-shaped AlN layer (b) EDX spectrum of the (a). Reprinted from Ref. [14] under the terms of Creative Commons CC-BY license.

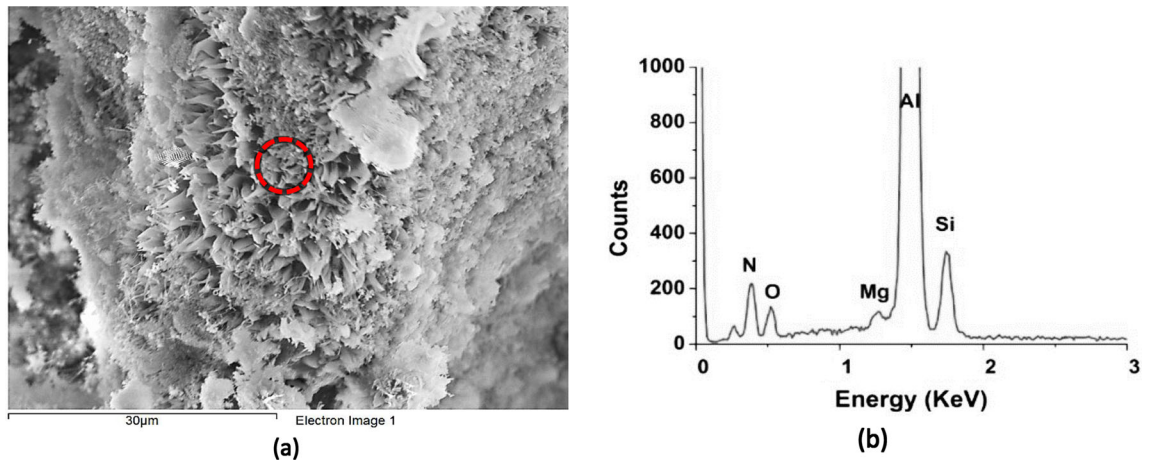


Fig. 7—(a) SEM micrograph of nitride on the fracture surface of un heat treated 2L99 + 0.4 wt pct Mo alloy (b) EDX spectrum and of the marked area in (a). Reprinted from Refs. [16,17].

close-packed planes between AlN and Al was 6.66 pct, indicating that AlN was a reasonably potent nucleating substrate for α -Al grains, having an *fr* of less than 7 pct. However, comparing the size of AlN with oxide and boride particles (MgAl_2O_4 , $\gamma\text{-Al}_2\text{O}_3$, TiB_2 , $\alpha\text{-Al}_2\text{O}_3$), Wang and Fan concluded that AlN particles were not as potent for nucleation as other particles in the melt.^[18]

This research aimed to investigate further the presence of AlN in an as-cast alloy, specifically Al-7Si-0.3Mg (2L99) and to study its morphology in both as-cast and laboratory-produced samples under an atmosphere of nitrogen. Understanding the morphology and prevalence of AlN in relation to bifilms is crucial as it is thought to have a considerable effect on the behavior of bifilms, perhaps more so than in the case of oxides^[13]

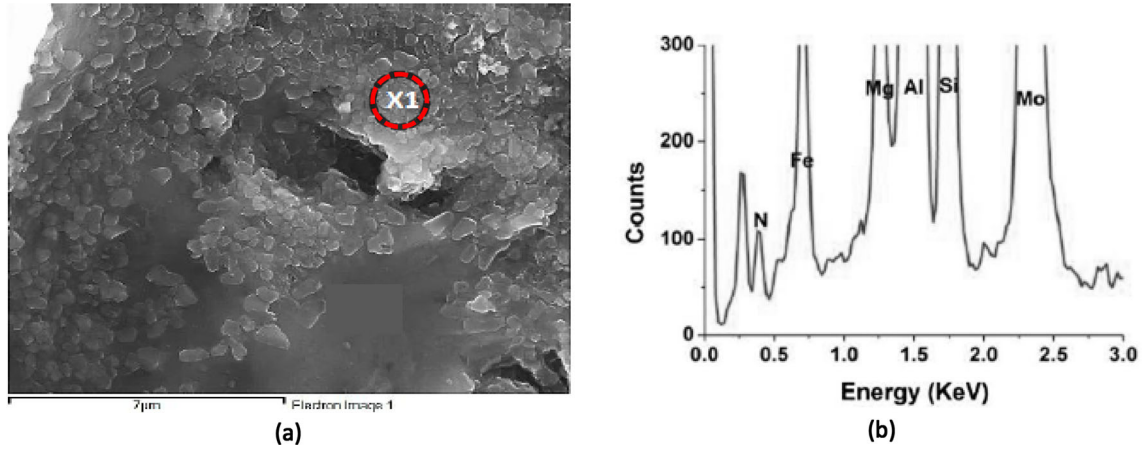


Fig. 8—(a) SEM micrographs of granular nitride layer on the surface of 2L99 + 0.4 wt pct Mo alloy, sample from the bubble-growth experiment. (b) EDX spectra of the marked area in (a). Reprinted from Refs. [16,17].

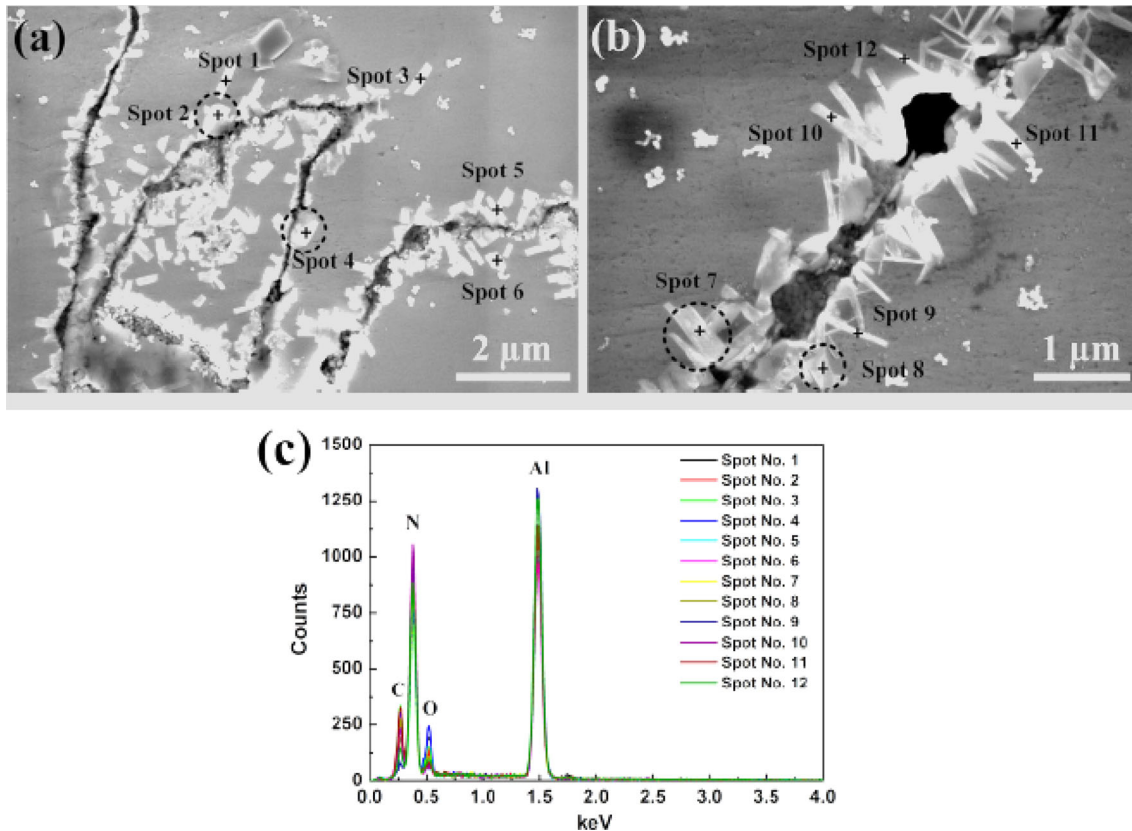


Fig. 9—(a) SEM micrograph of nitride inclusion particles held at (a) 750 °C and (b) 850 °C (c) the EDX spectrum of the marked areas and points in (a) and (b). Reprinted from Ref. [18].

Table I. Crystallographic Data of Al, AlN, and Common Oxides and Borides at 660 °C. Reprinted from Ref. [18]

Phase	Structure	Lattice Parameter		Close-Packed Plane	Close-Packed Row	$d_{(hkl)}$ (nm)	fd (Pct)	$r_{[uvw]}$ nm	fr (Pct)
		a	C						
Al	Cubic	0.4121	—	{111}	< 110 >	{111} 0.2379	N/A	0.2914	N/A
AlN	Hexagonal	0.3122	0.4992	{0001}	< 2110 >	{0002} 0.2496	4.67	0.3122	6.66
γ -Al ₂ O ₃	Cubic	0.7963	—	{111}	< 110 >	{222} 0.2299	3.50	0.2815	3.50
α -Al ₂ O ₃	Rhomb	0.4782	1.3057	{0001}	< 1100 >	{0006} 0.2176	9.33	0.2761	5.54
MgAl ₂ O ₄	Cubic	0.8126	—	{111}	< 110 >	{222} 0.2346	1.43	0.2873	1.43
TiB ₂	Hexagonal	0.3037	0.3237	{0001}	< 2110 >	{0001} 0.3237	26.49	0.3037	4.05

Table II. Composition of the 2L99, 2L99 + 0.6 wt pct Mo and 2L99 + 0.2 wt pct W Alloy

Element	Weight pct	Mo	W	Mg	Si	Fe	Ti	Cu	Zn	Pb	Sn	Al
2L99		0.00	0.00	0.3	9.8	0.03	0.14	0.00	0.00	0.00	0.00	Balance
2L99 + 0.6 wt pct Mo		0.64	0.00	0.32	8.55	0.06	0.11	0.00	0.00	0.00	0.00	Balance
2L99 + 0.2 wt pct W		0.00	0.21	0.29	9.42	0.14	0.00	0.00	0.00	0.00	0.00	Balance

through direct consumption of nitrogen or diffusion of hydrogen inside the bifilms. It is understood that this phenomenon has not been widely reported, and further research in this area is needed.

II. EXPERIMENTAL PROCEDURE

Initially, experiments were carried out to produce test bars cast in resin-bonded sand molds. The alloys used were based upon CP-Al, 2L99 alloy (Al-7Si-0.3Mg), 2L99 + 0.6 wt pct Mo, and 2L99 + 0.2 wt pct W reflecting the composition of alloys in which AlN had been detected in earlier work. The composition of the alloys is shown in Table II, measured by a BRUKER S8 Tiger wavelength-dispersive X-ray fluorescence (XRF) with a test duration of 7 minutes.

Grade 60 silica sand and (0.6 wt pct resin (types 5112 and 5230)) were used to make the sand molds. The running systems of the molds were deliberately badly designed with a long-running bar, and no filters to both encourage the creation of bifilms in the test bars due to surface turbulence and air entrapment in the melt, as shown in Figure 10.

The sand molds were made two weeks before casting to allow the evaporation of solvents from the resin-bonded sand molds, reducing hydrogen pick-up and gas porosity in the castings. Alloying elements Mo and W were used based on previous research. Chen^[17] reported that the addition of about 0.4 wt pct Mo and about 0.4 wt pct W brought about a beneficial effect on the mechanical properties of the alloys, specifically an improvement in the Weibull Modulus and a reduction

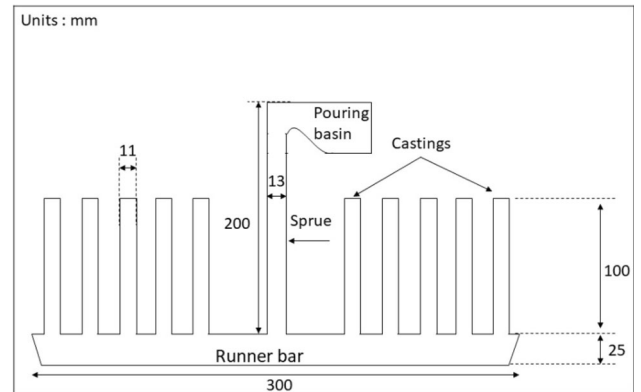


Fig. 10—Sketch of the “badly designed” running system. Reprinted from Ref. [16].

in the scatter of measured UTS values.^[17] This research reported in this paper aimed to determine the influence of Mo and W on AlN, if any.

Master alloys of nominal compositions 2L99 + 10 wt pct Mo and 2L99 + 10 wt pct W were made by the addition of 200 g of pure Mo, or 200 g of pure W, to 1800 g of 2L99 liquid metal carried out at a melt temperature of 1300 °C, held for 40 minutes before pouring the master alloy into a steel ingot mold.

Subsequently, 2 kg of 2L99 was melted in a C80 clay graphite crucible in a 175-kW induction furnace heated to 730 °C. Ar lance degassing was applied for 20 minutes to decrease the hydrogen content of the melt to less than 0.1 mm³/100 g, measured using a Severn Science hydrogen gas analyzer. Test bars from the sand molds,

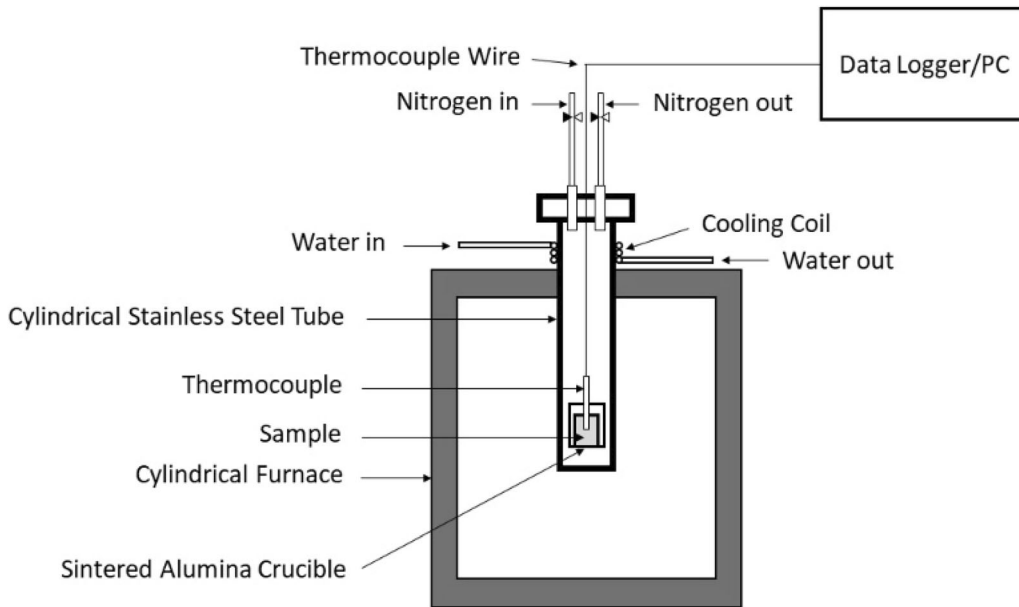


Fig. 11—Nitrogen growth experiment setup.

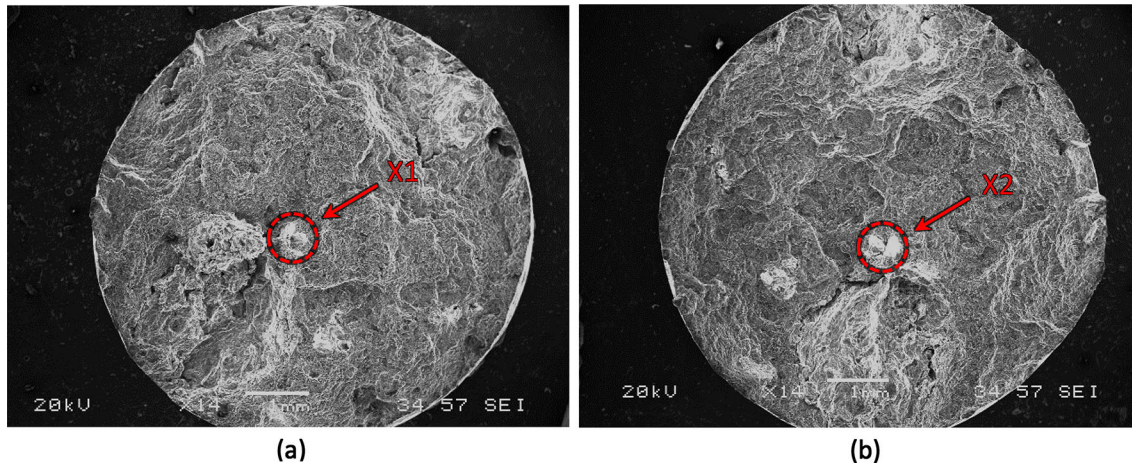


Fig. 12—(a) and (b) Low magnification of SEM micrographs of two halves of fracture surfaces of as-cast 2L99 test bar, showing bifilm defects and nitrides at the marked areas X1 and X2.

of composition 2L99 + 0.6 wt pct Mo and 2L99 + 0.2 wt pct W, were then cast by the addition of the master alloys, made as described above, to 2L99 liquid metal, with Ar lance degassing, cast at a melt temperature of 730 °C.

Each casting provided ten test bars of composition 2L99, 2L99 + 0.6 wt pct Mo and 2L99 + 0.2 wt pct W. These were machined to a standard size of 100 mm in length, with a gauge length of 37 mm and 26 mm radius on the gauge length. Tensile strength tests were conducted on 2L99 samples using a Zwick tensile strength testing machine carried out at 1 mm/min

strain rate. After breaking the 2L99 samples, each half of the broken test bar was cut 5 mm below the fracture surface and characterized using a Philips XL-30 FEG Environmental Scanning Electron Microscopy (SEM) equipped with an Inca Oxford Energy-Dispersive X-ray (EDX). It was reasonable to assume that the fracture surfaces represented the area with the largest concentration of defects; however, an additional study of AlN morphology on fracture surfaces was carried out using a Focused Ion Beam (FIB), dual beam FIB-SEM, equipped with an Electron-Dispersive X-ray.

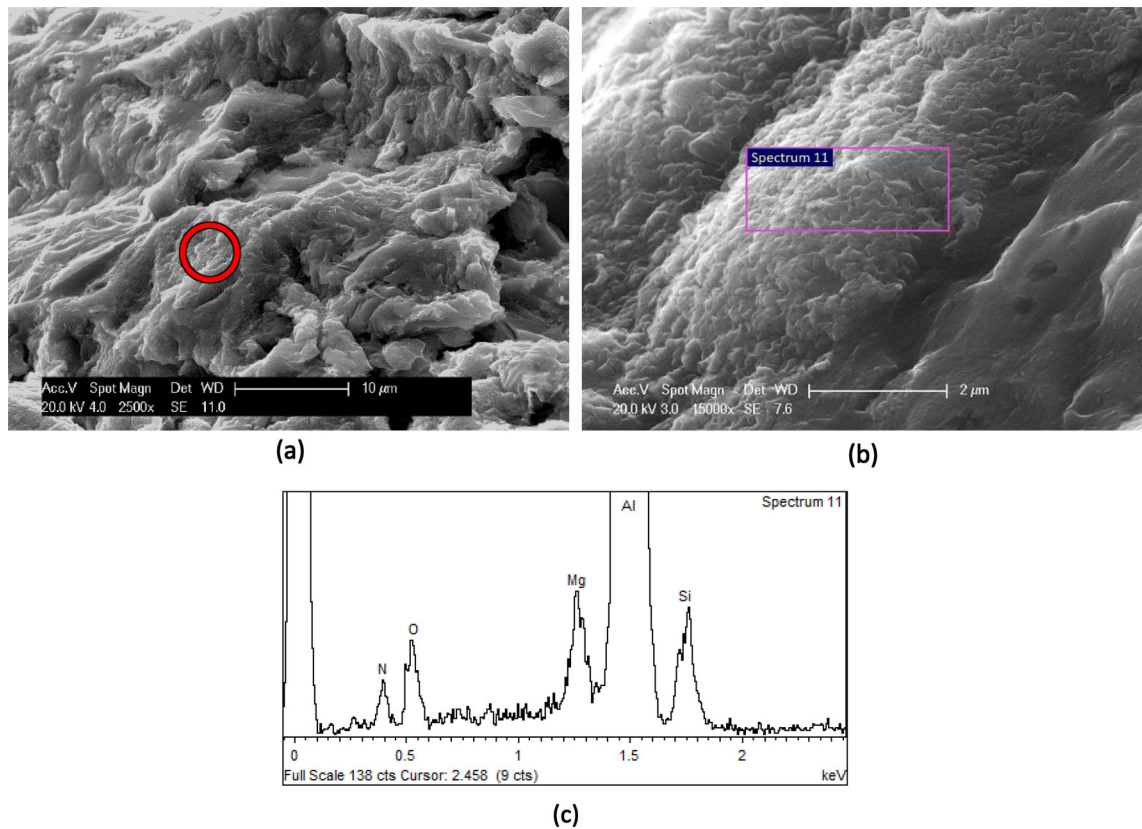


Fig. 13—(a) and (b) SEM micrograph of a layer of oxide and nitride on the fracture surface of as-cast 2L99 (c) EDX analysis of spectrum11 (the marked area) in (b).

In a separate experiment conducted to grow oxides and nitrides on CP-Al, 2L99, 2L99 + 0.6 wt pct Mo, and 2L99 + 0.2 wt pct W, the samples were held in a melt (see Figure 11), and cylindrical samples of diameter 15 mm and height 25 mm, were placed in a cylindrical sintered alumina crucible of 20 mm outer diameter, 16 mm inner diameter, and 30 mm in height. The crucibles were then inserted into a custom-made vertically oriented cylindrical stainless steel tube designed to allow control of the atmosphere of the melt (see Figure 11). The steel tube was placed inside a sealed vertical tube furnace, and the lid sealed with an O-ring and screws. An Inconel-sheathed Type-K thermocouple (0.5 mm diameter) was inserted through a valve into the tube and positioned adjacent to the crucible. Nitrogen gas was fed through a high-pressure tube to an inlet valve at a flow rate of $\sim 13 \text{ cm}^3/\text{min}$, while a high-pressure hose was connected to an outlet valve to discharge the nitrogen. The furnace was set to $850 \text{ }^\circ\text{C}$ and then held for 15 minutes to stabilize its temperature. The

sample was then held at various holding times of 1.5, 3, 6, 12, and 24 hours, after which the sample was left in the furnace to cool. The unaltered top surfaces of the samples undergoing growth and as recovered from the furnace were characterized using SEM.

III. RESULTS

A. Characterization of 2L99 Alloy at $730 \text{ }^\circ\text{C}$ (As-Cast) Conditions

Figures 12(a) and (b) show two halves of a test bar fracture surface of as-cast 2L99 alloy observed using SEM at low magnification. As mentioned in the experimental procedure, each half of the broken test bar was cut 5 mm below the fracture surface. High magnification and EDX results of areas marked X1 and X2 in Figures 12(a) and (b) are shown in Figures 13 and 14. The fracture surfaces revealed the presence of $220 \text{ }\mu\text{m}$ long bifilms, with small patches of aluminum

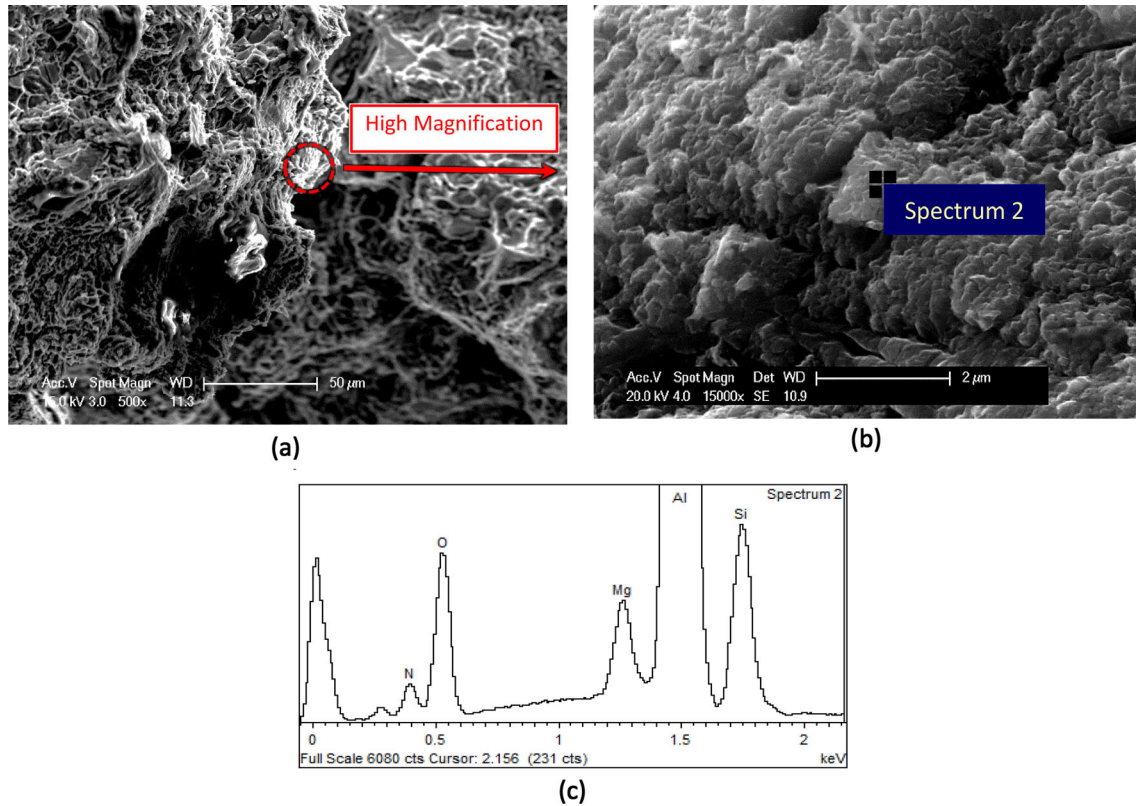


Fig. 14—(a) SEM micrograph showing a low magnification of the oxide layers and nitride on the fracture surface of 2L99 (as-cast condition) (b) higher magnification of SEM micrograph of the marked area in (a), (c) EDX analysis of spectrum2 of the marked area in (b).

Table III. Quantification of the Marked Area (Spectrum11) in Figure 13(b)

Description	Spectrum11 in Figure 13(b)	
	Weight pct	Atomic pct
N	12.54	20.39
O	10.04	14.29
Mg	1.43	1.34
Al	71.98	60.73
Si	4.01	3.25

Table IV. Quantification of the Market Area (Spectrum 2) in Figure 14(b)

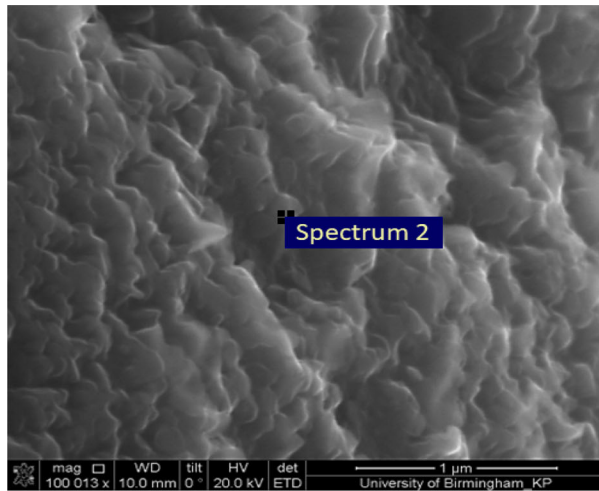
Description	Spectrum 2 in Figure 14(b)	
	Weight pct	Atomic pct
N	11.44	17.43
O	23.19	30.93
Mg	1.88	1.65
Al	56.25	44.49
Si	7.25	5.51

nitrides of about $15\ \mu\text{m}$ in length. This suggested symmetrical oxides and nitrides present on both halves of the fracture surfaces of the as-cast 2L99 alloy.

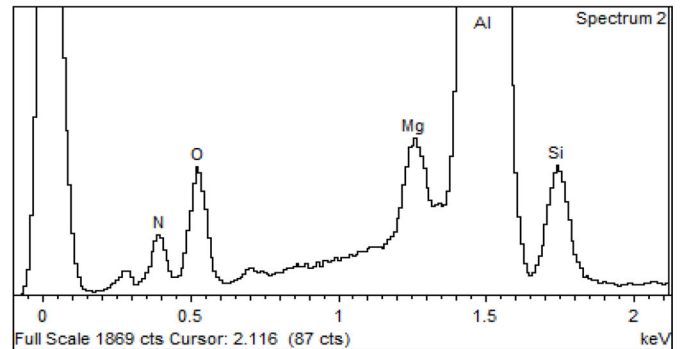
Figures 13(a) and (b) show the morphology and EDX quantification of nitride/oxide patches observed on a fracture surface of a 2L99 test bar (as marked in X1 in Figure 12(a)). The composition (Table III) for the marked area in Figure 13(b) confirms the presence of

oxides at 14 at pct and nitrides at 20 at pct. The nitride patches had a nodular shape and covered approximately $15\ \mu\text{m}$ of the fracture surface (Figure 13(b)).

The area marked in Figure 14(a) shows the area of nitride on the other half of the test bar marked X2 in Figure 12(b). Figure 14(b) shows a high-magnification image of the same marked area in Figure 14(a). Figure 14(c) is the EDX spectrum, and Table IV shows the quantification of spectrum 2 marked in Figure 14(b).

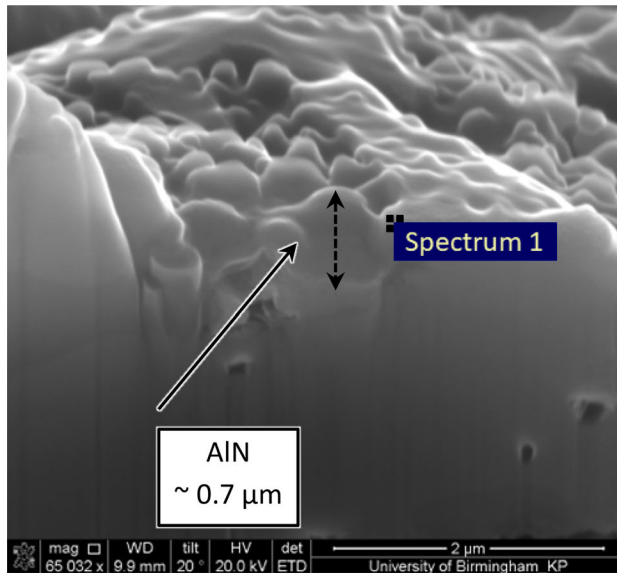


(a)

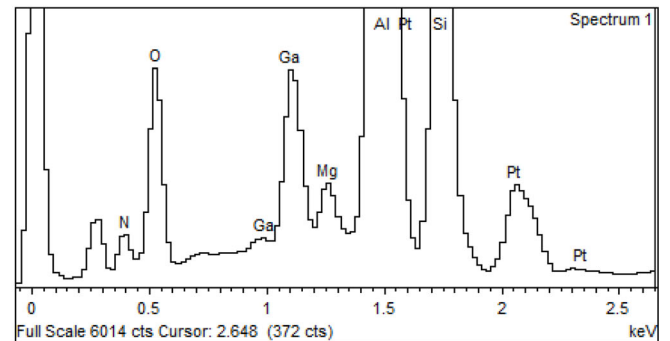


(b)

Fig. 15—(a) High magnification of SEM image of a nitride and oxide layer on the fracture surface of as-cast 2L99 and (b) EDX analysis of spectrum2.



(a)



(b)

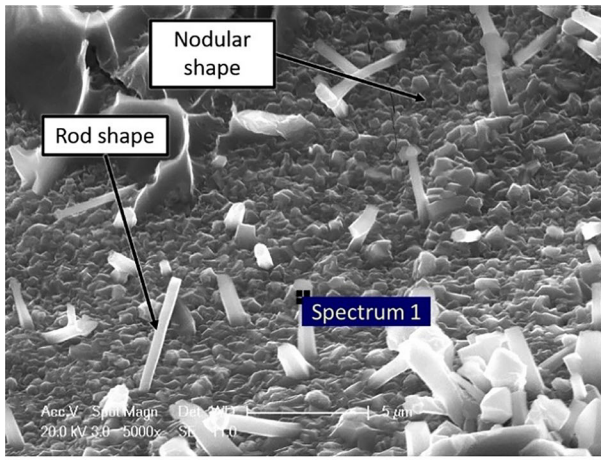
Fig. 16—(a) Cross-section of the nitride layer on the fracture surfaces of 2L99 (as-cast condition) without Pt coating (b) EDX analysis of Spectrum 1 showing both O and N as well as a small amount of Pt and Ga.

Table V. Quantification of the Marked Area (Spectrum 2) in Figure 15(b)

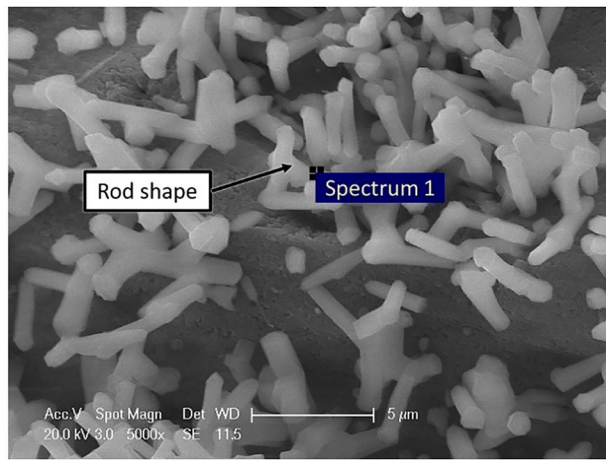
Description	Spectrum2 in Figure 15(a)	
	Weight pct	Atomic pct
N	10.93	17.95
O	10.53	15.13
Mg	1.02	0.96
Al	74.62	63.59
Si	2.90	2.38

Table VI. Quantification of the Marked Area (Spectrum 1) in Figure 16(b)

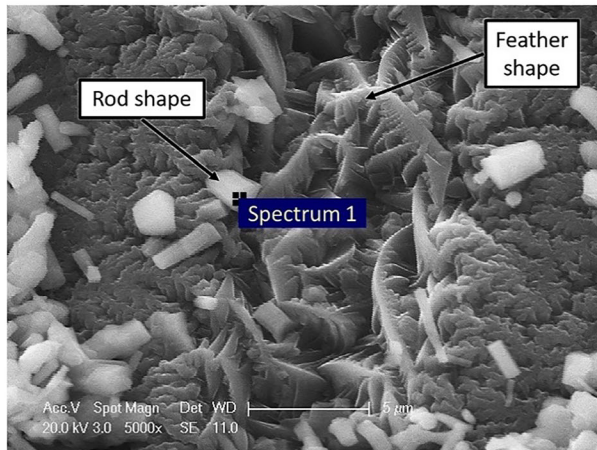
Description	Spectrum1 in Fig. 16(b)	
	Weight pct	Atomic pct
N	10.93	17.95
O	10.53	15.13
Mg	1.02	0.96
Al	74.62	63.59
Si	2.90	2.38
Ga	4.33	1.50
Pt	7.00	0.87



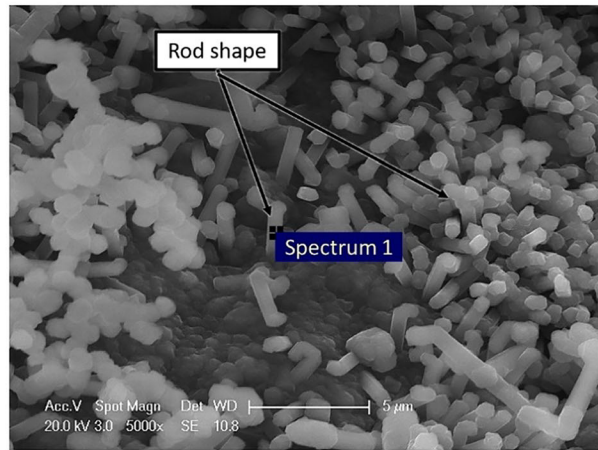
(a) CP- Al



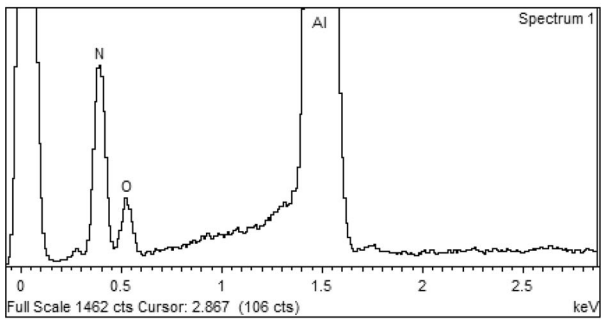
(b) 2L99



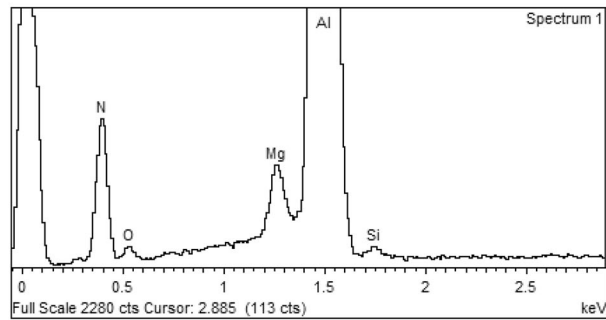
(c) 2L99+ 0.6 wt pct Mo



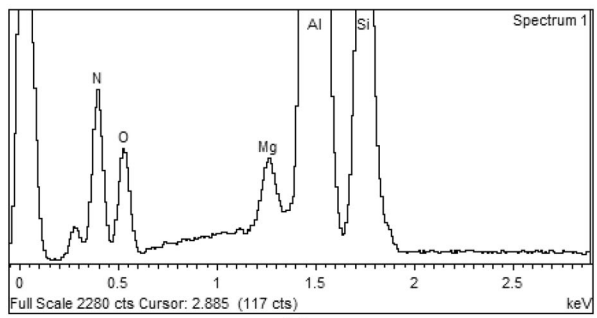
(d) 2L99+ 0.2 wt pct W



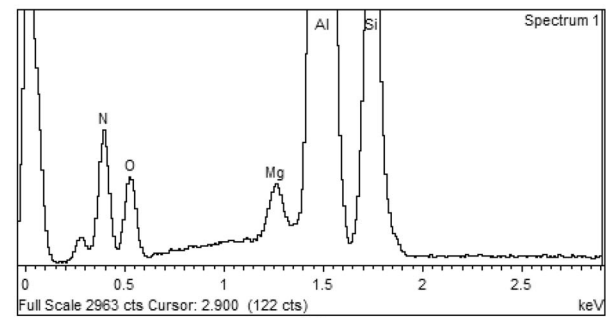
(e)



(f)



(g)



(h)

Fig. 17—(a) to (d) SEM micrographs of rod-shaped AlN on the surface of CP-Al, 2L99 alloy, 2L99 + 0.6 wt pct Mo alloy, and 2L99 + 0.2 wt pct W alloy, respectively, with 24 hours holding time in N at 850 °C. (e) to (h) EDX spectra for the marked areas shown in (a) to (d).

To more accurately define the shape and thickness of the nitride phases present on the fracture surface of the 2L99 alloy, the region represented in Figure 13(b) was investigated using FIB. Figure 15(a) displays a higher magnification of the nitride prior to milling, while Figure 16(a) shows the same area after milling, which was used to determine the nitride's thickness. This confirmed the nodular shape of AlN, where each nodule measured approximately 250 nm. Figure 14(b) shows the EDX analysis, and Table V shows the quantification of the spectrum2 for Figure 14(a).

Figure 16(a) shows the FIB cross-section of Figure 15(a). The thickness of the AlN layer was measured to be approximately 0.7 μm . Figure 16(b) shows an EDX analysis, and Table VI provides quantification of spectrum 1 as marked in Figure 15(a).

B. AlN Morphologies in the Nitrogen Growth Experiment

1. Rod-shaped AlN

Figures 17(a) through (h) show the micrographs and EDX spectra of rod-shaped nitrides with an average of 2 μm in width and about 6 μm in length. They were observed on the surfaces of all four different alloys, held for 24 hours in nitrogen gas. The largest rod shape, measured in CP-Al, was about $12 \times 2 \mu\text{m}$. Table VII shows the quantification of the spectra for Figures 17(a) through (d). The average dimensions of the rod-shaped AlN patches observed on the surface of the alloys examined were measured to be approximately 30 by 50 μm .

Feather-shaped AlN was also observed between the rod-shaped nitrides, as shown in Figure 17(c). The rod-shaped AlN appeared to be similar to that observed by Wang and Fan^[17] in CP-Al (see Figures 9(a) and (b)), although the latter was obtained from a polished cross-section.

2. Whisker-shaped AlN

Figures 18(a) through (h) show micrographs and EDX spectra of whisker-shaped nitrides on the surfaces of all four alloys, which were held for 12 hours in nitrogen. Exclusively to whisker shapes, the results from

the EDX spectra show the amount of O to be more than three times larger than the amount of N. Table VIII shows the quantification of spectra for Figures 18(a) through (d). The average dimensions of the whisker-shaped AlN patches observed on the surface of the alloys examined were measured to be approximately 60 by 90 μm .

C. Nodular-Shaped AlN

Figures 19(a) through (h) showed a nodular morphology obtained in a nitrogen atmosphere with a mean of approximately 250 nm. They were observed on the surfaces of all four alloys after holding for 3 hours in nitrogen. The nodular shapes were similar to those found in the as-cast condition described earlier (Figures 13(b), 14(a), 15(a) and 16(b)). Whisker-shaped nitrides were also observed occurring between the nodular-shaped nitrides (see Figure 19(a)). Table IX shows the quantification of the spectra for Figures 19(a) through (d). The average dimensions of the nodular-shaped AlN patches observed on the surface of the alloys examined were measured to be approximately 15 by 25 μm .

D. Feather-Shaped AlN

Figures 20(a) through (h) show micrographs and EDX spectra for feather-shaped nitrides with a mean dimension of around 10 μm in length, which ran through the central portion of the image (as marked). They covered an area of approximately $9 \times 38 \mu\text{m}$ of the surface. They were observed on the surfaces of all four alloys after being held for 6 hours in nitrogen. Table X shows the quantification of the spectra for Figures 20(a) through (d).

The average dimensions of the feather-shaped AlN patches observed on the surface of the alloys examined were measured to be approximately 15 by 30 μm .

The feather-shaped morphologies were similar to the findings of other researchers' AlN. Specifically, in the experiments reported involving 8 hours of holding time in the trapped air bubbles experiment,^[10-12] and on the fracture surfaces of 2L99 + 0.4 wt pct Mo in an as-cast

Table VII. Quantification of Spectra for Figure 17(a) through (d)

Description	Figure 17(a) Spectrum 1		Figure 17(b) Spectrum 1		Figure 17(c) Spectrum 1		Figure 17(d) Spectrum 1	
	Weight pct	Atomic pct	Weight pct	Atomic pct	Weight pct	Atomic pct	Weight pct	Atomic pct
N	33.35	47.29	35.94	51.20	29.92	41.96	29.92	41.96
O	7.20	8.94	2.65	3.31	14.60	17.92	14.60	17.92
Mg	0	0	1.10	0.90	0.92	0.75	0.92	0.75
Al	59.45	43.77	60.02	44.39	41.95	30.54	41.95	30.54
Si	0	0	0.29	0.21	12.61	8.82	12.61	8.82

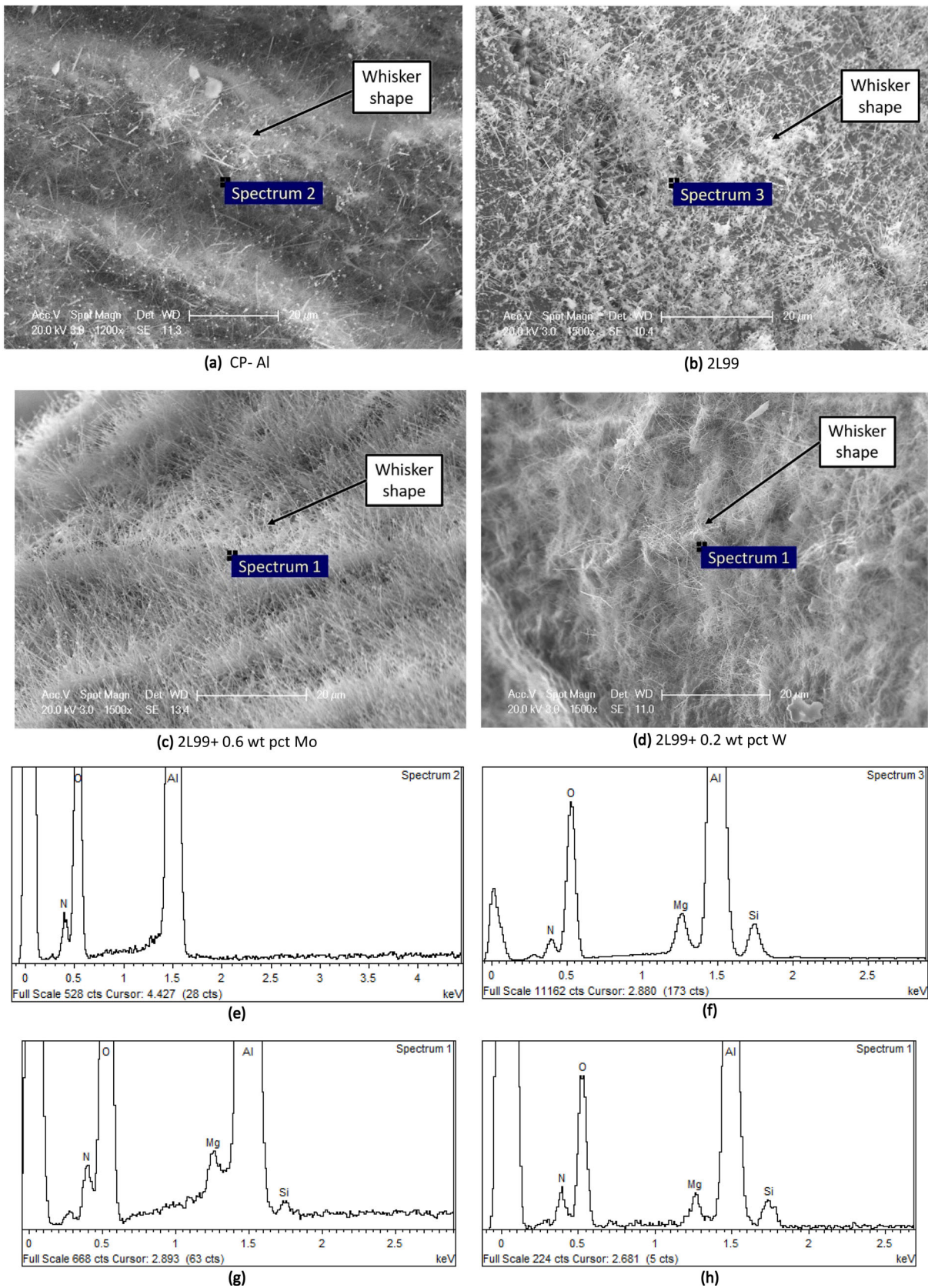


Fig. 18—(a) to (d) SEM micrographs of whisker-shaped AlN on the surfaces of CP-Al, 2L99 alloy, 2L99 + 0.6 wt pct Mo alloy, and 2L99 + 0.2 wt pct W alloy, respectively, with 12 hours of holding time in N at 850 °C; (e) through (h) EDX spectra for the marked areas shown in (a) through (d).

Table VIII. Quantification of Spectra for Figure 18(a) and (b)

Description	Figure 18(a) Spectrum 2		Figure 18(b) Spectrum 3		Figure 18(c) Spectrum 1		Figure 18(d) Spectrum 1	
	Weight pct	Atomic pct	Weight pct	Atomic pct	Weight pct	Atomic pct	Weight pct	Atomic pct
N	10.98	14.85	11.92	16.54	8.63	11.98	14.87	15.94
O	47.07	55.71	40.23	48.89	44.88	54.51	43.31	54.86
Mg	0	0	1.96	1.57	0.43	0.34	1.74	1.35
Al	41.94	29.44	43.29	31.20	45.87	33.04	37.91	26.40
Si	0	0	2.61	1.81	0.19	0.13	2.17	1.45

condition.^[16,17] In this study, a feather-shaped morphology was consistently observed in combination with other morphologies, such as the rod, whisker, and nodular morphologies. To summarize, the feather-shape morphology may be promoted by more extended holding periods (in this case, 6 hours) at 850 °C.

IV. DISCUSSION

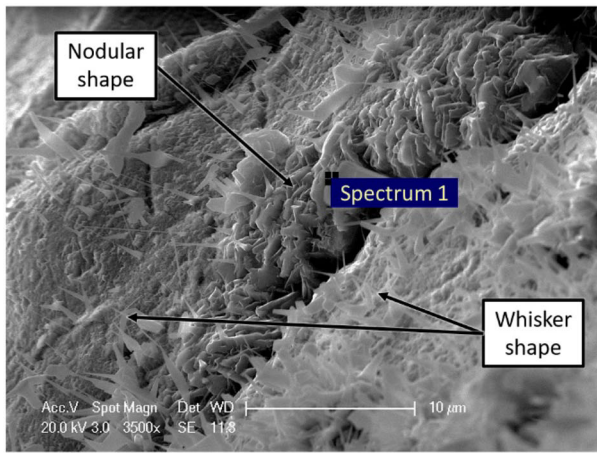
As shown in Figure 3 and on the eutectoid Al₂O₃-AlN phase diagram, AlON is not to be expected to occur at temperatures below 1640 °C. Therefore, the nitrogen detected by EDX has been concluded to be AlN, as the test bars were cast at 730 °C or were heated in the growth experiments at 850 °C.

For nucleation of AlN on Al, and other Al oxide substrates, there should be a small difference between lattice size and structure. Interatomic spacing misfit f_r is fundamental to grain refinement and nucleation, with an optimal f_r (calculated interatomic spacing misfit) difference of 7 pct being suggested.^[18] The interatomic spacing misfit between AlN and Al oxides was calculated based on the crystallographic data as shown in Table I.^[18] The interatomic spacing misfit was calculated to be 10.9 pct for γ -alumina, 13.1 pct for α -alumina, and 8.7 pct for spinel, all of which were greater than the value of 7 pct as mentioned above. This suggests that AlN may not be a potent substrate for Al oxide nucleation, in contrast with Wang and Fan's research^[18] as well as this research's observations, which showed AlN may nucleate on oxide particles confirmed by EDX analysis detecting both O and N elements, as shown in Figures 9(c), 13(c), 14(b), 15(b), and 16(c).

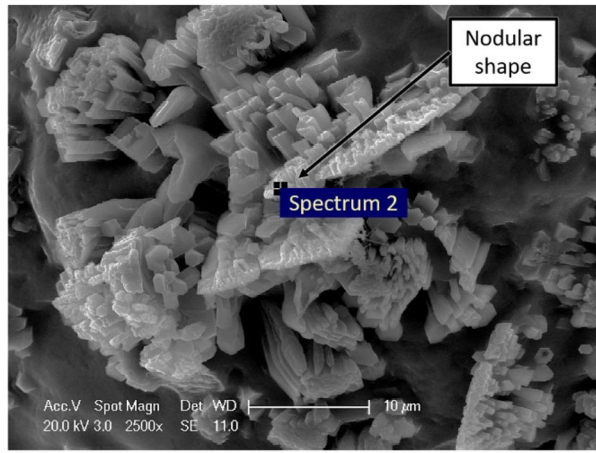
In previous research, a feather-shaped AlN morphology was found on the surface of pure Al^[10-12] and on the fracture surfaces of 2L99 + 0.4 wt pct Mo^[16,17] but not on the fracture surfaces of 2L99 test bars. Based on Chens' observations of the patches of AlN on the fracture surfaces of 2L99 + 0.4 wt pct Mo, it was suspected that AlN might have formed at high temperatures (1300 °C) in the production of the master alloy, to be carried through to the as-cast test bars. However, in this research, no evidence of AlN was observed in the characterization of ten test bars of 2L99 + 10 wt pct Mo and ten test bars of 2L99 + 10 wt pct W master alloys.

In this research, AlN has been found, for the first time, on the fracture surfaces of a 2L99 alloy in the as-cast condition at 730 °C rather than in laboratory experiments. The AlN particles observed were nodular and appeared to be impermeable. This is in contrast with previously observed AlN particles in samples cast in different conditions,^[11,12,16,17] which have been described as feather-shaped and appeared to be more permeable (as shown in Figures 5(a), 6(a), and 7(a)). Table XI shows a summary of the different nitrides observed by other researchers, created under laboratory conditions.

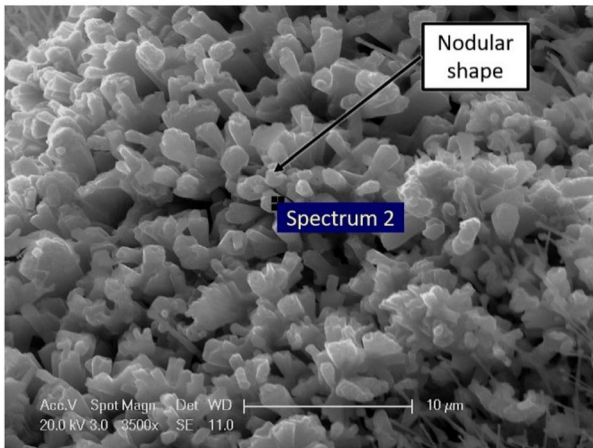
The most impermeable AlN phase observed in this research, in the as-cast condition, is suggested to be of a nodular morphology. In this case, AlN may act as a hindrance to the passage of reaction gases between the entrapped atmosphere of a bifilm and the surrounding liquid metal. The impermeable AlN layer may also lead to a reduction in hydrogen diffusion through the bifilm preventing further expansion of the bifilm, supporting the Nyahumwa hypothesis.^[2,17]



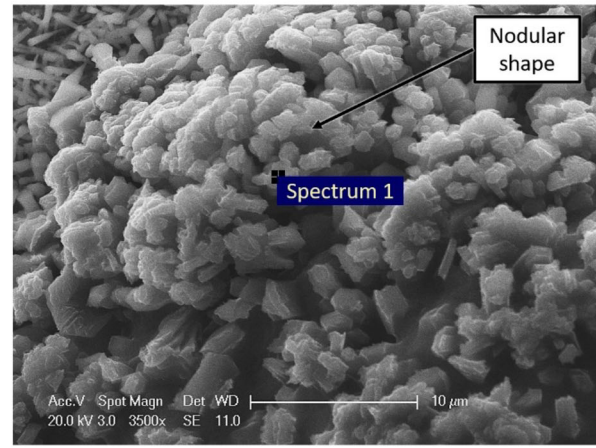
(a) CP- Al



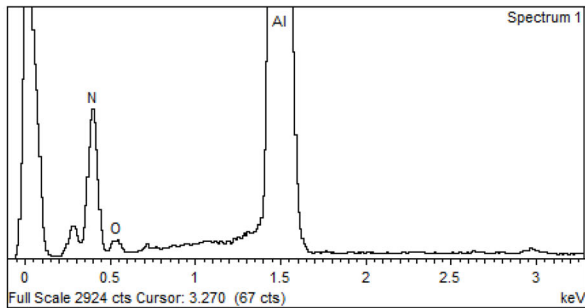
(b) 2L99



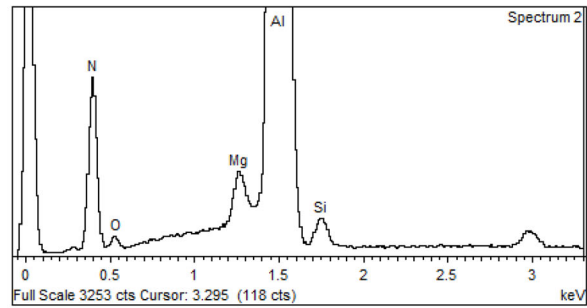
(c) 2L99+0.6 wt pct Mo



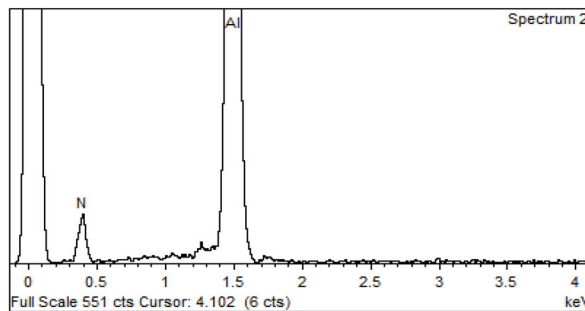
(d) 2L99+0.2 wt pct W



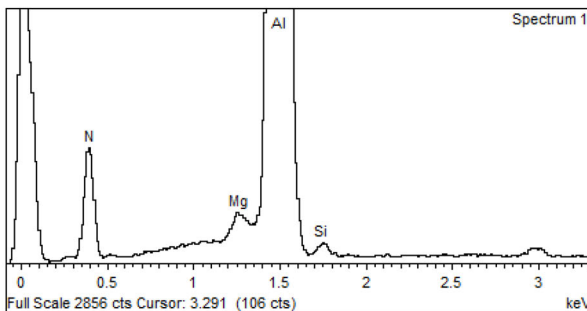
(e)



(f)



(g)



(h)

Fig. 19—(a) to (d) SEM micrographs of nodular-shaped AlN on the surfaces of CP-Al, 2L99 alloy, 2L99 + 0.6 wt pct Mo alloy, and 2L99 + 0.2 wt pct W alloy, respectively, with 3 hours of holding time in N at 850 °C; (e) to (h) EDX spectra of the marked areas shown in (a) to (d).

Table IX. Quantification of Spectra for Figures 19(a) and (b)

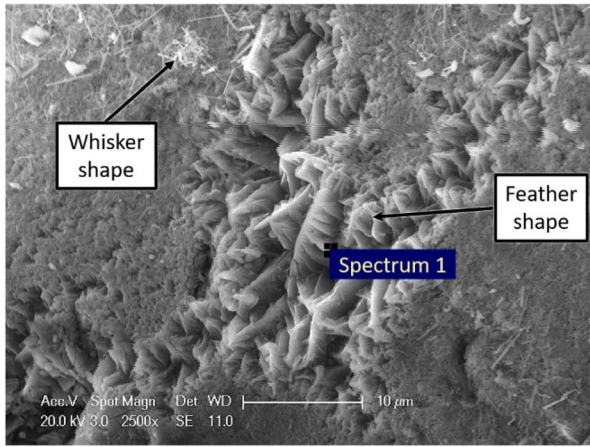
Description	Figure 19(a) Spectrum3		Figure 19(b) Spectrum1		Figure 19(a) Spectrum3		Figure 19(b) Spectrum1	
	Weight pct	Atomic pct	Weight pct	Atomic pct	Weight pct	Atomic pct	Weight pct	Atomic pct
N	42.41	57.54	35.94	51.36	37.82	53.95	36.34	52.36
O	3.94	4.68	2.15	2.69	0	0	0	0
Mg	0	0	0.64	0.53	0	0	0.44	0.37
Al	53.65	37.78	60.43	44.83	62.18	46.05	62.76	46.94
Si	0	0	0.84	0.60	0	0	0.46	0.33

The AlN phase in this study showed them to be of various morphologies, such as rod, nodular, feather, and whisker. These morphologies were observed in all Al alloys of CP-Al, 2L99, 2L99 + 0.6 wt pct Mo, and 2L99 + 0.2 wt pct W, with different holding times and in small patches rather than over the entire surface, as presented in section B of this paper. No consistent pattern of AlN distribution was observed. The nitrogen growth experiments showed the existence of AlN in all the alloys examined at every holding period.

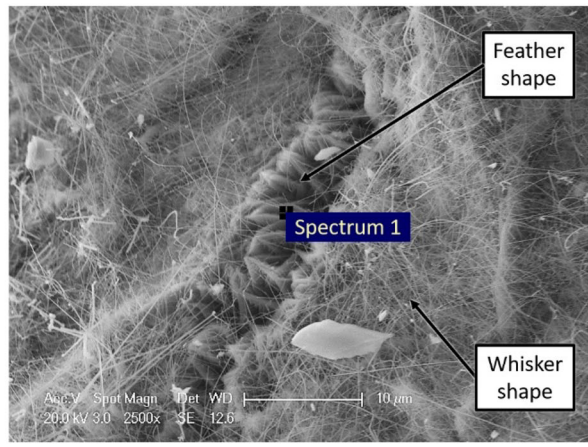
The observed morphologies of AlN particles suggested that the feather-shaped AlN particles were more readily formed in the CP-Al alloy than in the 2L99, 2L99 + 0.6 wt pct Mo and 2L99 + 0.2 wt pct W alloys. This may have been caused by the lack of the alloying elements Si and Mg in CP-Al. It was challenging to observe the feather and nodular-shaped AlN in all alloys, while the rod and whisker-shaped morphologies were more frequently observed. The feather-shaped morphology was generally found sandwiched between either rod or whisker-shaped morphologies, as shown in Figures 20(a) through (d). Nodular and rod-shaped AlN were found to occur alone and with whisker or feather-shaped AlN on the fracture surfaces, as shown in Figures 19(a) through (d) and Figures 17(a) through (d), whereas whisker-shaped morphology was observed alone, as shown in Figures 18(a) through (d).

V. CONCLUSIONS

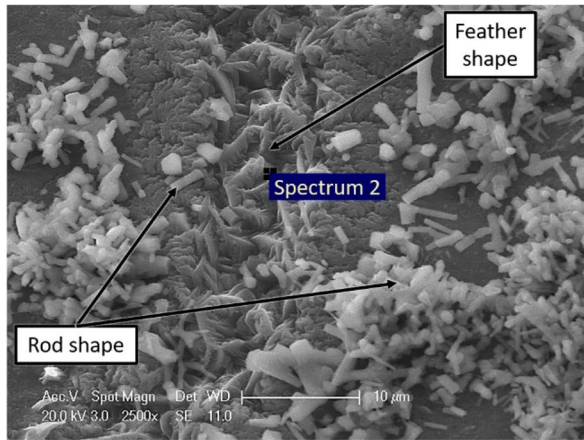
1. Four AlN morphologies were observed after various holding times under nitrogen gas in all the different Al alloys such as CP-Al, 2L99, 2L99 + 0.6 wt pct Mo, and 2L99 + 0.2 wt pct W. These were rod, whisker, nodular, and feather-shaped.
2. Nodular AlN particles were observed in as-cast alloy conditions on the fracture surfaces of 2L99 alloy, measuring approximately 15 μm in length. Observation of AlN particles in as-cast alloy conditions supports Nyahumwa's *et al.* hypothesis^[2] of consumption of the gases within the bifilms and the presence of nitrides in the process.
3. The presence of nodular nitrides observed in as-cast conditions in this study suggests (i) the consumption of oxygen within the bifilms, (ii) nucleation of nitrides and their growth, as Nyahumwa *et al.*^[2] suggested, and (iii) a possible role for hydrogen within the bifilms, depending on whether there was a considerable hydrogen content in the solution in the liquid metal. These considerations may result in a notable difference in the bifilm size and a change in the mechanical properties of the alloys.



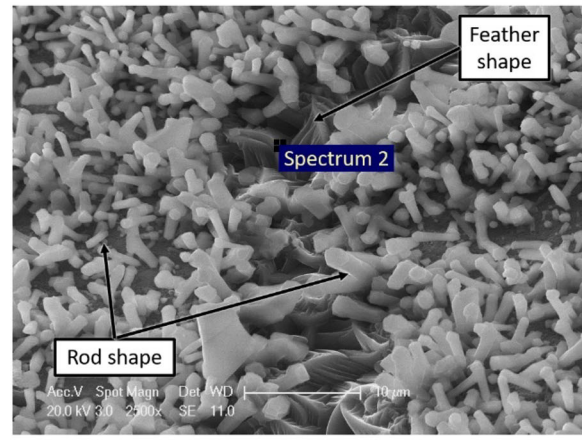
(a) CP-Al



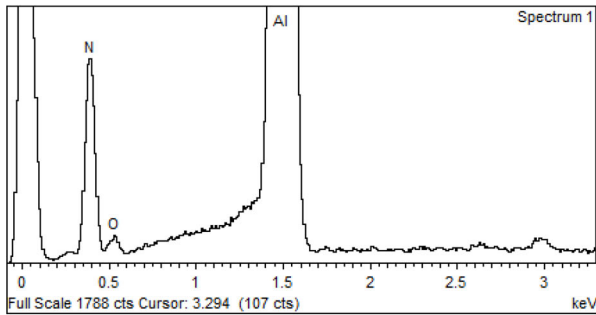
(b) 2L99



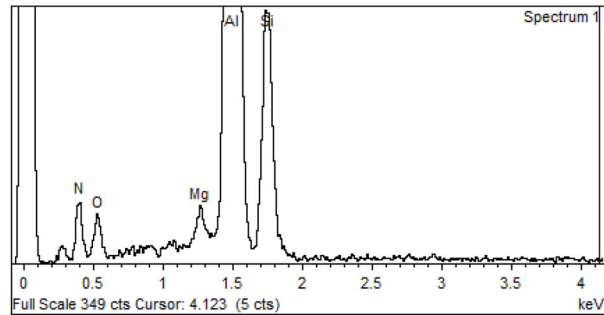
(c) 2L99+0.6 wt pct Mo



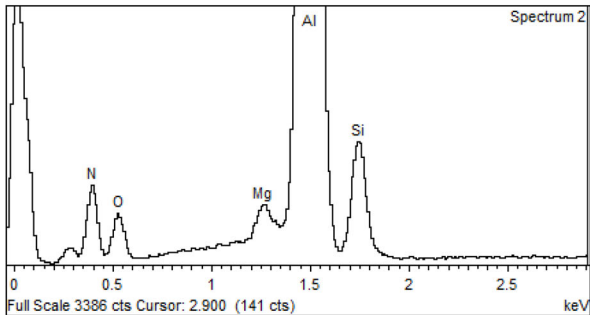
(d) 2L99+0.2 wt pct W



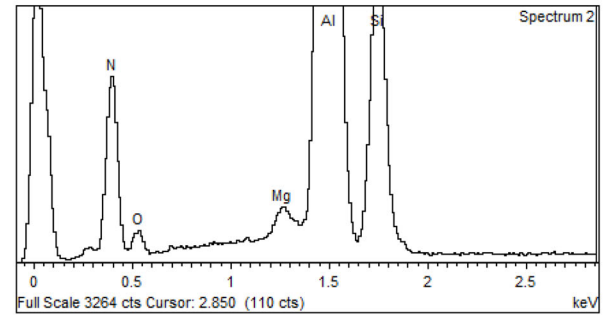
(e)



(f)



(g)



(h)

Fig. 20—(a) to (d) SEM micrographs of feather-shaped AlN on the surfaces of CP-Al, 2L99 alloy, 2L99 + 0.6 wt pct Mo alloy, and 2L99 + 0.2 wt pct W alloy, respectively, with 6 hours holding time in N at 850 °C; (e) through (h) EDX spectra of the marked areas shown in (a) through (d).

Table X. Quantification of Spectra for Figures 20(a) and (b)

Description	Figure 20(a) Spectrum2		Figure 20(b) Spectrum1		Figure 20(a) Spectrum2		Figure 20(b) Spectrum1	
	Weight pct	Atomic pct	Weight pct	Atomic pct	Weight pct	Atomic pct	Weight pct	Atomic pct
N	37.66	53.04	24.20	36.13	24.98	37.15	42.01	56.93
O	2.73	3.36	10.18	13.31	9.46	12.32	5.18	6.15
Mg	0	0	0.74	0.64	0.67	0.57	0.48	0.38
Al	59.61	43.59	52.69	40.84	60.01	46.34	43.12	30.33
Si	0	0	12.20	9.08	4.89	3.62	9.21	6.22

Table XI. Summary of Different AlN Morphologies Found by Other Researchers, Mainly in Pure Al and 2L99 + 0.4 wt pct Mo

Researcher	Alloy	Temperature	Holding Time	Morphology	AlN Weight/ atomic pct	Width
Raeiszadeh ^[10–12]	Pure Al	850 °C	8 Hours	Feather-shaped	28 wt pct	—
Gerrard ^[13, 14]	Pure Al	700 °C	15 minutes	Feather-shaped	17 wt pct	8.6 μm
Chen ^[16, 17]	2L99 + 0.4wt pctMo	730 °C	N/A (fracture surface, as-cast alloy)	Feather-shaped	36 at pct	15 μm
Wang and Fan ^[18]	CP-Al	750 to 850 °C	N/A (Pressure melt filtration technique)	Rod-shaped	—	104 nm

ACKNOWLEDGMENTS

The authors wish to acknowledge the financial support of the EPSRC (grant reference EP/L016206/1). The authors also would like to thank Mr. Adrien Caden and Mr. Jonathan Davies from the School of Metallurgy and Materials, the University of Birmingham, for their technical assistance in this research work. The authors would also like to thank Ms. Theresa Morris and Dr Ludwig Schneider for their assistance in the operation of the various Scanning Electron Microscopes in the department.

CONFLICT OF INTEREST

The authors declare that they have no conflict of interest.

OPEN ACCESS

This article is licensed under a Creative Commons Attribution 4.0 International License, which permits use, sharing, adaptation, distribution and reproduction in any medium or format, as long as you give appropriate credit to the original author(s) and the source, provide a link to the Creative Commons licence, and indicate if changes were made. The images or other third party material in this article are included in the article's Creative Commons licence, unless indicated otherwise in a credit line to the material. If material is not included in the article's Creative Commons licence

and your intended use is not permitted by statutory regulation or exceeds the permitted use, you will need to obtain permission directly from the copyright holder. To view a copy of this licence, visit <http://creativecommons.org/licenses/by/4.0/>.

REFERENCES

1. J. Campbell: *Castings*, 2nd ed. Butterworth-Heinemann, Oxford, 2001, pp. 17–67.
2. C. Nyahumwa, N.R. Green, and J. Campbell: *AFS Trans.*, 1998, vol. 106, pp. 215–23.
3. H.X. Willems, M.M.R.M. Hendrix, G. de With, and R. Metselaar: *J. Eur. Ceram. Soc.*, 1992, vol. 10, pp. 339–46.
4. H.X. Willems, M.M.R.M. Hendrix, R. Metselaar, and G. de With: *J. Eur. Ceram. Soc.*, 1992, vol. 10, pp. 327–37.
5. S.A. Impey, D.J. Stephenson, and J.R. Nicholls: *Mater. Sci. Technol. (United Kingdom)*, 1988, vol. 4(12), pp. 1126–32.
6. M.A. El-Sayed, H.G. Salem, A.Y. Kandeil, and W.D. Griffiths: *Metall. Mater. Trans. B*, 2014, vol. 45B(4), pp. 1398–06.
7. Q. Zheng, B. Wu, and R.G. Reddy: *Adv. Eng. Mater.*, 2003, vol. 5, pp. 167–72.
8. N. Nagendra, B.S. Rao, and V. Jayaram: *Mater. Sci. Eng. A.*, 1999, vol. 269, pp. 26–37.
9. Q. Zheng and R.G. Reddy: *J. Mater. Sci.*, 2004, vol. 39, pp. 141–49.
10. R. Raeiszadeh: PhD Thesis, University of Birmingham, UK, 2005.
11. R. Raeiszadeh, and W.D. Griffiths: Conf. on Estimation of the Duration of the Atmosphere Within a Double Oxide Film Defect in Pure Aluminum, The University of Birmingham, UK, 2005, pp. 464–71.
12. R. Raeiszadeh and W.D. Griffiths: *Metall. Mater. Trans. B.*, 2006, vol. 37B, pp. 865–71.
13. A.J. Gerrard: PhD Thesis, University of Birmingham, UK, 2014.
14. W.D. Griffiths, A.J. Gerrard, and Y. Yue: Conference on Oxide film defects in Al alloys and the formation of hydrogen-related porosity, Materials Science and Engineering. The University of

Birmingham, UK, 2016.

15. W.D. Griffiths, A. Elsayed, and M.A. El-Sayed: *Metall. Mater. Trans. B.*, 2016, vol. 47B, p. 3459.
16. Q. Chen and W.D. Griffiths: *Metall. Mater. Trans. B.*, 2021, vol. 52B, pp. 502–16.
17. Q. Chen: PhD Thesis, University of Birmingham, UK, 2017.

18. F. Wang and Z. Fan: *Metall. Mater. Trans. A*, 2019, vol. 50A, pp. 2519–26.

Publisher's Note Springer Nature remains neutral with regard to jurisdictional claims in published maps and institutional affiliations.